JPEDAV (2005) 26:23-38
DOI: 10.1361/15477030522455
1547-7037/$19.00 ©ASM International

Thermodynamic Modeling of the Fe-S System

P. Waldner and A.D. Pelton

(Submitted October 20, 2003; in revised form November 15, 2004)

A thorough review and critical evaluation of phase equilibria and thermodynamic data for all phases in the iron-sulfur (Fe-S) binary system at 1 bar pressure has been made over the entire composition range for temperatures from 25 °C to above the liquidus. The Gibbs energies of ten phases have been modeled, and optimized model parameters have been obtained that reproduce all data simultaneously within experimental error limits. For the liquid phase, the recently extended modified quasi-chemical model is applied for the first time to a liquid metal-sulfur phase. A two-sublattice model within the framework of the compound energy formalism is used for the high-temperature monosulfide pyrrhotite solution. A substitutional model is used for the dissolution of S in solid iron. The Gibbs energies of six stoichiometric compounds are also modeled.

1. Introduction

Systems of transition metals and sulfur play an important role in the fields of materials science (hot corrosion) and metallurgical research (smelting processes), as well as in geochemistry and cosmochemistry. The binary iron-sulfur (Fe-S) system represents a key subsystem in developing an extended thermodynamic database of multicomponent metal-S systems.

At elevated temperatures, the Fe-S system contains two complex condensed solution phases with extended homogeneity ranges (Ref 1). These are a liquid phase showing a continuous transition from metallic to sulfidic character and a monosulfide phase with hexagonal NiAs structure melting congruently around 1190 °C. The liquidus on the Fe-rich side of the phase diagram is quite flat, indicating a tendency to metastable demixing into Fe-rich and sulfide-rich liquids. At elevated pressures, a wide miscibility gap between a liquid matte and a S-rich supercritical fluid dominates the S-rich side of the phase diagram. The monosulfide, or pyrrhotite, phase $Fe_{1-x}S$, exhibits a substantial deviation from stoichiometry toward excess S. There is general agreement in the literature on phase relations involving pyrrhotite at higher temperatures. However, below 320 °C the stability relations among various superstructure phases are very complex and still not completely elucidated (Ref 2, 3). A series of iron sulfides with structures related to the NiAs structure, and extending from stoichiometric FeS (troilite) to a composition close to Fe_7S_8 (denoted in the literature as monoclinic pyrrhotite), have been reported in numerous publications as the so-called pyrrhotite group. These superstructure phases arise by the clustering of metal atoms in the troilite structure and the ordering of metal atoms and vacancies in more metal-deficient compositions. At room temperature, three stoichiometric superstructure compounds, $Fe_{11}S_{12}$, $Fe_{10}S_{11}$, and Fe_9S_{10}, are known in addition to troilite and monoclinic pyrrhotite (Ref 4). Only tentative phase diagrams below 320 °C for compositions between FeS and Fe_7S_8, involving $Fe_{11}S_{12}$, $Fe_{10}S_{11}$, and Fe_9S_{10}, are presented in the literature (Ref 3, 4). The most S-rich compound is the disulfide (pyrite). It is stable up to approximately 743 °C, at which point it melts incongruently to high-temperature pyrrhotite $Fe_{1-x}S$ and almost pure liquid S (Ref 1).

The Fe-S system has been thermodynamically modeled by Hillert and Staffansson (Ref 5), who calculated the partial phase diagram for Fe-FeS, treating high-temperature pyrrhotite as the stoichiometric compound FeS. Sharma and Chang (Ref 6) modeled the thermodynamic properties of the liquid phase and calculated the phase diagram. An associated solution model was used to describe the Gibbs energy of the liquid. An associated "FeS" species was assumed in addition to Fe and S. For the pyrrhotite phase, a defect thermodynamic model, based on the study by Libowitz (Ref 7), taking into account Fe interstitials and vacancies, was used. Guillermet et al. (Ref 8) presented an assessment of the entire Fe-S system using two-sublattice models for the liquid phase and the pyrrhotite phase. The solubility of S in the solid-Fe phases was treated by a regular solution model. Pyrite was modeled as stoichiometric. Chuang et al. (Ref 9) reevaluated the Fe-S system on the basis of more recent data that were available at the time. The same models as in their earlier work (Ref 6), with different model parameters, were used for the liquid and the solid monosulfide phases. The austenite and ferrite phases were treated as Henrian solutions. Pyrite was taken to be stoichiometric. Kongoli et al. (Ref 10) used the modified quasi-chemical model for short-range ordering to describe the liquid Fe-S solution over the composition range from pure metal to matte. Only phase equilibria between pure Fe and the modeled liquid phase were presented. Solid sulfide phases were not modeled. No phase equilibria below 320 °C have been taken into account by any of the studies cited above.

Due to the scientific and industrial importance of metal-S systems in metallurgy, materials science, and geological science, thermodynamic modeling over the entire composition range from pure metal to pure S is required. Consequently,

P. Walder and **A.D. Pelton,** Centre de Recherche en Calcul Thermochimique, École Polytechnique de Montréal, P.O. Box 6079, Station "Downtown" Montréal, QC H3C 3A7, Canada. Contact e-mail: apelton@polymtl.ca.

the aim of the present modeling study is to cover the whole composition range from 25 °C to above the liquidus temperatures. For the analytical description of the Gibbs energy of the Fe-S liquid phase, the recently improved modified quasi-chemical model is applied for the first time to a metal-S liquid phase. S solubility in all solid-Fe phases as well as the homogeneity range of high-temperature pyrrhotite are taken into consideration. Due to the lack of, and uncertainties in, experimental information on the exact phase relations between the various pyrrhotite superstructures below 600 K, no attempt has been made to model the ordering effects of vacancies in the pyrrhotite solid solution at low temperatures. However, for the first time all stoichiometric superstructure compounds between troilite and monoclinic pyrrhotite reported in the literature have been modeled consistently with the thermodynamic properties of high-temperature pyrrhotite.

2. Experimental Data

Two major groups of experimental information were used for modeling calculations in this work. One group consisted of *T-X* (temperature-composition) phase diagram data, including data on phase boundaries and information on invariant reactions. The other group consisted of experimental thermodynamic information such as enthalpies of mixing or S activities, for both single-phase and two-phase regions.

2.1 Phase Diagram Data

The modeling calculations were based on the general features of the phase diagram assessment carried out by Kubaschewski (Ref 1), in which a review of phase diagram data in the literature obtained by various experimental techniques (e.g., metallography, thermal analysis, and x-ray analysis) is given. In the current study, experimental data from the original articles and data from publications (Ref 11-33) not quoted in the review are used for comparison with the modeling results. Phase boundary data derived from experimental thermodynamic quantities are also used (Ref 15-18, 34-42).

2.2 Thermodynamic Data

Various experimental techniques have been applied to study the thermodynamic properties of the Fe-S system. Due to the very large amount of published work, a selective citation is necessary to provide a broad and representative compilation. In the following paragraphs, the articles are quoted in chronological order for each experimental method.

Several publications have reported enthalpies of mixing involving the liquid phase. Vaisburd et al. (Ref 43) investigated calorimetrically enthalpies of S dissolution in liquid Fe at 1600 °C. Iguchi et al. (Ref 44) used an isoperibol calorimeter at steelmaking temperatures to measure the heat of mixing of liquid Fe-S solutions. Kanda et al. (Ref 45) measured heat contents with a drop calorimeter in the composition range 0.38 to 0.5 S mole fraction over the temperature range 670 to 1233 °C. Sudavtsova et al. (Ref 46) studied the thermochemical properties of liquid melts with an isoperibol calorimeter.

Electromotive force (emf) measurements also have been reported. Oishi et al. (Ref 47) carried out thermodynamic studies by a galvanic cell technique with CaF_2 solid electrolytes at temperatures between 612 and 805 °C. Ramanarayanan and Worrell (Ref 48) used CaF_2 solid electrolytes in the body-centered cubic (bcc)-(Fe)/pyrrhotite region in the temperature range 500 to 900 °C. Ono and Moriyama (Ref 49) used galvanic cells involving solid CaS electrolytes doped with Y_2S_3 for the determination of chemical potentials of S in the Fe-rich region of the Fe-S system between 1000 and 1300 °C. Mehrotra and Wagner (Ref 50) studied the thermodynamic properties of pyrrhotite in the temperature range 600 to 1000 °C using galvanic cells with the configuration Pt, air/YSZ/$Fe_{1-x}S$, Fe_3O_4, SO_2 (1 atm), Pt (where YSZ stands for yttria-stabilized zirconia).

The majority of the thermodynamic data in the literature were obtained by equilibration with H_2S/H_2 gas mixtures. Sherman et al. (Ref 51) determined the thermodynamic properties of S dissolved in liquid steel at S concentrations up to 4.8 wt.% by equilibration with H_2/H_2S mixtures between 1530 and 1730 °C. Using the same method, Bog and Rosenqvist (Ref 52) and Ban-ya and Chipman (Ref 53) determined S activities at 1120 °C, and between 1500 and 1600 °C, respectively, for S contents up to 7.2 wt.%. Alcock and Cheng (Ref 54) equilibrated small beads of pure metals and alloys with H_2/H_2S mixtures of controlled ratio at 1540 °C. The S content of the beads was analyzed by the oxygen-combustion method. Activity-composition relationships for Fe-S melts have been established by Nagamori et al. (Ref 16) between 1000 and 1300 °C. Bale and Toguri (Ref 18) used a thermogravimetric technique to measure directly the composition of the liquid phase in equilibrium with H_2/H_2S gas mixtures at 1200 °C. Hayashi and Uno (Ref 55) determined the activity of S in liquid Fe by equilibrating liquid Fe and H_2S/H_2 gas mixtures using a resistance furnace at 1500 and 1600 °C. Resistance and induction furnaces were used by Ishii and Fuwa (Ref 56) at 1500 to 1650 °C. Mattes were equilibrated with gaseous H_2/H_2S mixtures at 1250 °C by Koh and Yazawa (Ref 57). Fe-S melts in the temperature range between 1550 and 1650 °C were the subject of an article by Baren and Gokcen (Ref 58).

Kapustin and Bryukvin (Ref 59) evaluated S vapor pressures by thermogravimetric analysis of the desulfuration rates of Fe-S melts under flowing inert gas between 1000 and 1500 °C.

The dewpoint method was used by Ditman and Vechko (Ref 35), who measured the vapor pressure of S above that of sulfides close to the composition of FeS between 1000 and 1400 °C. Schürmann and Henke (Ref 36) applied the same method to study the saturation vapor pressure of S between 1200 and 1600 °C at a total pressure of 1 atm.

Some work has been carried out to study simultaneously S activities and the solubility of S in the low- and high-temperature modifications of Fe. Rosenqvist and Dunicz (Ref 38) studied the solubility of S in α-, γ- and δFe. Gas

mixtures of controlled H_2/H_2S ratios were passed over pure metallic Fe heated to a temperature in the range 900 to 1500 °C. The amount of S absorbed by the Fe was determined by chemical analysis. Turkdogan et al. (Ref 39) equilibrated H_2/H_2S mixtures and metal samples followed by an analysis of each sample for S. The solubility of S in austenite was thus determined to be between 1000 and 1335 °C. Herrnstein et al. (Ref 40) measured the S solubility in ferrite in the temperature range 750 to 890 °C by equilibration with H_2/H_2S atmospheres. Fischer and Schwerdtfeger (Ref 41) reacted Fe platelets with gas phases of controlled H_2/H_2S ratios. After quenching, S contents were analyzed chemically. From the results, S potentials and S solubilities were established in the temperature range 1100 to 1300 °C.

Margot et al. (Ref 42) used a radiochemical method between 950 and 1250 °C that permitted them to determine the solubility of S in equilibrium with H_2/H_2S gas mixtures.

Numerous studies on S activities in $Fe_{1-x}S$ have been published. Among the most comprehensive investigations are those of Burgmann et al. (Ref 15) and Rau (Ref 37). Burgmann et al. (Ref 15) investigated the equilibrium of Fe-S samples in the composition range of pyrrhotite with H_2/H_2S gas mixtures between 700 and 1300 °C. S potentials in pyrrhotite and in the liquid phase were also reported. Rau (Ref 37) measured S fugacities in equilibrium with pyrrhotite at various temperatures from 550 to 1100 °C by equilibration with H_2S/H_2 mixtures and by a direct method using silica pressure gages. Lin et al. (Ref 60) and Hsieh (Ref 61) equilibrated the iron sulfide with gas mixtures consisting of H_2 and H_2S in the temperature range from 700 to 900 °C. The corresponding compositions of the sulfide phase were calculated from the weight change during the experiments.

Finally, several publications reported data mainly for two- or three-phase regions. One of the most comprehensive studies on the Fe-S system was carried out by Rosenqvist (Ref 62), who studied the thermodynamics of iron sulfides at temperatures between 400 and 1200 °C by equilibration with H_2S/H_2 mixtures and by S pressure measurements using the dewpoint method. Turkdogan (Ref 63) also used the H_2S/H_2 equilibration method to determine S activities as a function of composition in ferrous sulfides at 670, 800, and 900 °C, whereas the study by Nagamori (Ref 17) was performed in the temperature range between 700 and 900 °C.

Merwin and Lombard (Ref 24) determined the dissociation pressure of pyrite in the framework of a broad study of the system Fe-Cu-S, presenting data for the pyrite/pyrrhotite equilibrium. Sudo (Ref 64) investigated the equilibrium during the reduction of solid ferrous sulfide to Fe by H gas using a flow method between 775 and 872 °C. Toulmin and Barton (Ref 29) used the electrum-tarnish method to study the interrelations among pyrrhotite composition, S fugacity, and temperature. Vapor pressures related to the pyrite/pyrrhotite equilibrium were determined at temperatures in the range 325 to 743 °C. Ferro et al. (Ref 65) studied the sublimation behavior of pyrite by vapor pressure measurements using a simultaneous torsion-Knudsen apparatus.

3. Thermodynamic Modeling

The thermodynamic modeling of the Gibbs energies of every phase in the system is developed by critical evaluation and the optimization of experimental data. Several semiempirical models exist that provide analytical expressions of Gibbs energies as functions of temperature and composition. In a thermodynamic "optimization," adjustable model parameters are calculated simultaneously using all available thermodynamic and phase equilibrium data to obtain one set of model equations as functions of temperature, pressure, and composition. From these equations, all of the thermodynamic properties and phase diagrams can be back-calculated. The data are thereby rendered self-consistent and consistent with thermodynamic principles.

Thermodynamic data, such as activities, can aid in the evaluation of the phase diagrams, and the information on phase equilibria can be used to deduce thermodynamic properties. Thus, it is frequently possible to resolve discrepancies in the available data, and all interpolations and extrapolations can be made in a thermodynamically correct manner. A small set of model parameters is obtained, which is ideal for computer storage. They can be used to recalculate all thermodynamic properties as well as an optimized version of the corresponding phase diagram. Furthermore, the model equations for the various phases in binary systems then can be used with the models to predict the properties of multicomponent systems containing these binaries as subsystems.

There are few experimental thermodynamic and phase equilibria data available for pressures other than approximately 1 bar. Consequently, pressure dependence is only taken into consideration for the Gibbs energy of the gas phase based on the assumption of ideal gaseous solutions.

3.1 Gas Phase

For the thermodynamic description of the gas-phase constituents, S species from S_1 to S_8 as well as gaseous Fe and FeS are taken into account. At 1 bar total pressure, the gas phase becomes stable in the technologically important composition regions of the system at temperatures above ~1000 °C. Consequently, the Gibbs energy expression for an ideal gaseous solution model was accepted:

$$G = \sum_{i \geq 1} X_i G_i^{\circ} + RT \sum_{i \geq 1} (X_i \ln X_i) \qquad \text{(Eq 1)}$$

where G_i° represents the standard Gibbs energies of the corresponding pure gaseous phase constituents, X_i are the mole fractions of the constituents, R is the gas constant, and T is the absolute temperature.

3.2 The Liquid Phase

For the analytical description of the Gibbs energy of the liquid phase, a new version (Ref 66) of the well-established modified quasi-chemical model (Ref 67) is applied for the first time to a metal-S liquid phase. In the new version (Ref 66), the energy of nearest-neighbor pair formation is ex-

panded as a polynomial in the pair fractions, rather than in the component fractions, as was previously the case (Ref 67). In addition, the nearest-neighbor "coordination numbers" are now allowed to vary with composition. These modifications provide greater flexibility in fitting the binary data and in combining optimized binary systems into large databases for multicomponent solutions (Ref 68).

Liquid metal sulfide solutions exhibit a high degree of short-range ordering resulting from the fact that metal-S nearest-neighbor pairs are energetically favored over metal-metal and S-S pairs. In particular, in the system Fe-S, at compositions around 50 mol% S, this strong ordering results in a change of S potential of several orders of magnitude over a narrow composition range, with an inflection point near 50 mol% S. Simple empirical expansions of the excess thermodynamic properties as polynomials in the component mole fractions, as are often used to describe molten alloys, do not provide an adequate description for liquid sulfide solutions. "Associate models," which assume the existence of moleculelike species, are better than simple polynomial models and can correctly describe the observed curves of S partial pressure as a function of composition in binary metal-S systems. However, because such models are not physically realistic, they do not give good predictions of the properties of ternary and multicomponent solutions from the optimized binary parameters and require several empirical ternary and quaternary model parameters to reproduce the properties of multicomponent solutions.

The recently improved modified quasi-chemical model (Ref 66) used here gives a more realistic description of short-range ordering in liquid metal-S solutions. The atoms Fe and S are distributed over the sites of a quasi-lattice. The following pair exchange reaction is considered:

$$(\mathrm{Fe}-\mathrm{Fe})+(\mathrm{S}-\mathrm{S})=2(\mathrm{Fe}-\mathrm{S}) \qquad \text{(Eq 2)}$$

where (Fe-S) represents a first-nearest-neighbor pair. The nonconfigurational Gibbs energy change for the formation of two moles of Fe-S pairs according to Eq 2 is Δg_{FeS}. The analytical description of the Gibbs energy is given by:

$$G=(n_{\mathrm{Fe}}G^{\mathrm{o}}_{\mathrm{Fe}}+n_{\mathrm{S}}G^{\mathrm{o}}_{\mathrm{S}})-T\Delta S^{\mathrm{config}}+(n_{\mathrm{FeS}}/2)\Delta g_{\mathrm{FeS}} \qquad \text{(Eq 3)}$$

where $G^{\mathrm{o}}_{\mathrm{Fe}}$ and $G^{\mathrm{o}}_{\mathrm{S}}$ are the molar Gibbs energies of the pure components, $\Delta S^{\mathrm{config}}$ is the configurational entropy of mixing given by a random distribution of the (Fe-Fe), (S-S), and (Fe-S) pairs (Ref 66) in the one-dimensional Ising approximation, n_{Fe} and n_{S} are the numbers of moles of Fe and S atoms, and n_{FeS} is the number of moles of Fe-S pairs.

When the model parameter Δg_{FeS} is negative, Eq 2 is displaced to the right, with (Fe-S) pairs being favored. The "equilibrium constant" of the "quasi-chemical reaction" (Eq 2) becomes larger as Δg_{FeS} becomes more negative. At 50 mol% S, the melt contains mainly (Fe-S) pairs. At S contents below 50 mol%, the melt contains principally (Fe-S) and (Fe-Fe) pairs. Δg_{FeS} is expanded as a polynomial in terms of the pair fractions $X_{\mathrm{FeFe}}=n_{\mathrm{FeFe}}/(n_{\mathrm{FeFe}}+n_{\mathrm{SS}}+n_{\mathrm{FeS}})$ and $X_{\mathrm{SS}}=n_{\mathrm{SS}}/(n_{\mathrm{FeFe}}+n_{\mathrm{SS}}+n_{\mathrm{FeS}})$, where n_{FeFe}, n_{SS}, and n_{FeS} are the numbers of moles of each kind of pairs:

$$\Delta g_{\mathrm{FeS}}=\Delta g^{\mathrm{o}}_{\mathrm{FeS}}+\sum_{i\geq 1} g^{i0}_{\mathrm{FeS}}X^{i}_{\mathrm{FeFe}}+\sum_{j\geq 1} g^{0j}_{\mathrm{FeS}}X^{j}_{\mathrm{SS}} \qquad \text{(Eq 4)}$$

where $\Delta g^{\mathrm{o}}_{\mathrm{FeS}}$, g^{i0}_{FeS}, and g^{0j}_{FeS} are the adjustable model parameters that can be functions of temperature. When the Fe-rich melts (with <50 mol% S) contain mainly (Fe-Fe) and (Fe-S) pairs, X_{SS} is small in this composition range, and so the parameters g^{0j}_{FeS} have little influence. Similarly, in melts containing > 50 mol% S, X_{FeFe} is small, and the parameters g^{i0}_{FeS} have little influence. Hence, the two composition regions can be modeled nearly independently. This represents an improvement over the previous version of the model (Ref 67), where Δg_{FeS} was expanded as a polynomial in X_{S}, and, as a result, all model parameters affected the entire composition range, thereby making it more difficult to obtain a satisfactory optimization as well as generally necessitating a larger number of parameters.

The second change to the original modified quasi-chemical model is that the "coordination numbers" of Fe and S, Z_{Fe} and Z_{S}, can now vary with composition:

$$\frac{1}{Z_{\mathrm{Fe}}}=\frac{1}{Z_{\mathrm{FeFe}}}\left(\frac{2n_{\mathrm{FeFe}}}{2n_{\mathrm{FeFe}}+n_{\mathrm{FeS}}}\right)+\frac{1}{Z_{\mathrm{FeS}}}\left(\frac{n_{\mathrm{FeS}}}{2n_{\mathrm{FeFe}}+n_{\mathrm{FeS}}}\right) \qquad \text{(Eq 5)}$$

$$\frac{1}{Z_{\mathrm{S}}}=\frac{1}{Z_{\mathrm{SS}}}\left(\frac{2n_{\mathrm{SS}}}{2n_{\mathrm{SS}}+n_{\mathrm{FeS}}}\right)+\frac{1}{Z_{\mathrm{SFe}}}\left(\frac{n_{\mathrm{FeS}}}{2n_{\mathrm{SS}}+n_{\mathrm{FeS}}}\right) \qquad \text{(Eq 6)}$$

where Z_{FeFe} is the value of Z_{Fe} when all nearest neighbors of an Fe atom are Fe atoms, and Z_{FeS} is the value of Z_{Fe} when all nearest neighbors are S atoms. Z_{SS} and Z_{SFe} are defined in an analogous manner. The composition of maximum short-range ordering is thus determined by the ratio $(Z_{\mathrm{FeS}}/Z_{\mathrm{SFe}})$, which, in the present case, is set at 1 to 1. Values of the binary coordination numbers Z_{FeS} and Z_{SFe} are unique to the Fe-S binary system, while the values of the unary coordination numbers Z_{FeFe} and Z_{SS} are common to all systems containing Fe or S as a component. This gives greater flexibility in treating multicomponent solutions compared with the previous version of the model (Ref 67) in which Z_{FeS} and Z_{SFe} were necessarily equal to Z_{FeFe} and Z_{SS}, respectively.

3.3 Iron Solid Solutions: fcc-Iron and bcc-Iron

Assuming a random substitutional solid solution of S in the face-centered cubic (fcc) (γFe) and bcc (α- and δFe) modifications of Fe, the following Gibbs energy expression is applicable for both solution phases:

$$G=X_{\mathrm{Fe}}G^{0}_{\mathrm{Fe}}+X_{\mathrm{S}}G^{0}_{\mathrm{S}}+\mathrm{RT}(X_{\mathrm{Fe}}\ln X_{\mathrm{Fe}}+X_{\mathrm{S}}\ln X_{\mathrm{S}})+G^{\mathrm{ex}} \qquad \text{(Eq 7)}$$

where G^{0}_{Fe} is the standard Gibbs energy of the corresponding pure solid Fe phase, and G^{0}_{S} is the standard Gibbs energy

of pure hypothetical solid S with fcc or bcc structure. The G_S^0 values are model parameters. G^{ex} is an excess Gibbs energy that describes the first-nearest-neighbor interaction energies between Fe and S atoms as a function of temperature and composition. A Redlich-Kister expression was chosen to describe the composition dependence:

$$G^{ex} = X_S X_{Fe} \sum_{n\geq 0} {}^{n}L_{(Fe,S)}(X_S - X_{Fe})^n \quad \text{(Eq 8)}$$

where ${}^{n}L_{(Fe,S)}$ are the adjustable model parameters that can be functions of T.

3.4 High-Temperature Pyrrhotite

The crystal structure of the high-temperature pyrrhotite phase $Fe_{1-x}S$ is of the $B8_1$ type (Pearson symbol *hP*4, space group $P6_3/mmc$) (Ref 69). The S atoms form a close-packed hexagonal (cph) arrangement in which the octahedral voids are occupied by Fe atoms. This phase exhibits a wide homogeneity range extending from FeS stoichiometry to ~0.55 mol fraction S. Hägg and Sucksdorff (Ref 22) showed that the deviation from stoichiometry (metal deficiency) results from Fe vacancies in the lattice. Two sublattices can be distinguished in the crystal lattice: $(Fe,Va)_1(S)_1$. The first sublattice, the octahedral positions, contains Fe atoms and vacancies (Va). The second sublattice is the cph array of S atoms. Guillermet et al. (Ref 8) used this two-sublattice approach for the thermodynamic assessment of $Fe_{1-x}S$. Libowitz (Ref 7), and subsequently Sharma and Chang (Ref 6) and Chuang et al. (Ref 9), assumed Frenkel defects in their modeling studies (i.e., in addition to Fe vacancies, also Fe on interstitial sites). In terms of a sublattice notation, as noted above, this requires an additional sublattice according to $(Fe,Va)_1(Fe,Va)_1(S)_1$. It should be noted that such a model would correspond to a crystal structure of the $B8_2$-type (Pearson symbol *hP*6, space group $P6_3/mmc$), sometimes also designated as a "filled" NiAs-type. However, such a model with additional adjustable parameters is only justified when there is sufficient experimental evidence, as for example in the case of the $B8_2$ phase in the system indium-nickel, which was modeled by Waldner and Ipser (Ref 70). As is shown in Section 4, and in a subsequent article on the modeling of ternary Fe-Ni-S pyrrhotite, all presently available experimental data for high-temperature pyrrhotite can be very well described by the two-sublattice model. Consequently, no additional interstitial metal sublattice is introduced in the current study.

Table 1 Optimized excess Gibbs energy parameters of the liquid phase (in J/mol)

$\Delta g^{\circ}_{FeS} = -104{,}888.10 + 0.338\ T$
$g^{10}_{FeS} = +35{,}043.32 - 9.880\ T$
$g^{20}_{FeS} = +23{,}972.27$
$g^{30}_{FeS} = +30{,}436.82$
$g^{01}_{FeS} = +8626.26$
$g^{02}_{FeS} = +72{,}954.29 - 26.178\ T$
$g^{04}_{FeS} = +25{,}106$

For the analytical description of the Gibbs energy of high-temperature pyrrhotite, the compound energy formalism derived by Hillert and Staffansson (Ref 71), and generalized by Sundman and Ågren (Ref 72), was chosen. It yields the expression for the Gibbs energy of the $Fe_{1-x}S$ phase:

$$G = y_{Fe}G^0_{FeS} + y_{Va}G^0_{VaS} + RT(y_{Fe}\ln y_{Fe} + y_{Va}\ln y_{Va}) + G^{ex} \quad \text{(Eq 9)}$$

where y_{Fe} and y_{Va} are the site fractions of Fe and vacancies on the metal sublattice, respectively, G^0_{FeS} is the Gibbs energy of defect-free stoichiometric FeS, and G^0_{VaS} is the

Table 2 Optimized enthalpies of formation relative to elemental S in its most stable state at 298.15 K, absolute third-law entropies at 298.15 K, and excess Gibbs energy parameters of the bcc and fcc Fe solid solutions

Model compound	$\Delta_f H_{298.15}$, J/mol	$S_{298.15}$, J/(mol · K)
bcc-(S)	+24,954.78	46.377
fcc-(S)	+66,082.63	22.444
Excess Gibbs energy parameters, J/mol		
bcc solid solution	${}^0L = -31{,}041.003 - 10.657\ T$	
fcc solid solution	${}^0L = -59{,}070.736 - 34.612\ T$	

Table 3 Optimized model parameters for high-temperature pyrrhotite

Model compound	$\Delta_f H_{298.15}$, J/mol	$S_{298.15}$, J/(mol · K)
$(Fe)_1(S)_1$	−96,291.00	69.429
$(Va)_1(S)_1$	+140,049.39	32.054
Excess Gibbs energy parameters		
${}^0L_{(Fe,Va:S)} = -225{,}830.67 + 26.359\ T$		

Note: Enthalpies of formation are relative to the elements in their most stable states at 298.15 K. $S_{298.15}$ of $(Va)_1(S)$, is estimated as equal to the entropy of pure orthorhombic S at 298.15 K (Ref 76).

Table 4 Optimized enthalpies of formation relative to the elements in their most stable states at 298.15 K and absolute third-law entropies at 298.15 K of the stoichiometric compounds in the Fe-S system

Compound	$\Delta_f H_{298.15}$, J/mol	$S_{298.15}$, J/(mol · K)
FeS (troilite)	−100,121.00	60.31
$Fe_{11}S_{12}$	−1,148,081.30	755.18
$Fe_{10}S_{11}$	−1,048,475.20	693.00
Fe_9S_{10}	−950,758.00	623.50
$Fe_{7.016}S_8$ (monoclinic pyrrhotite)	−755,384.00	486.32
FeS_2 (pyrite)	−171,048.03	52.93

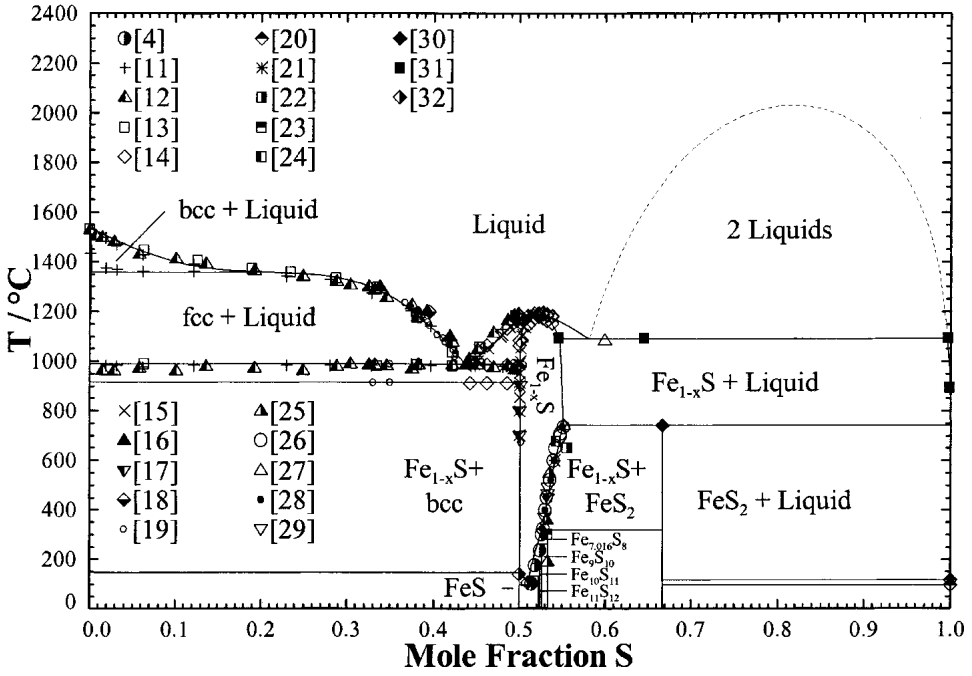

Fig. 1 Calculated, optimized, condensed Fe-S phase diagram together with experimental data

Table 5 Heat-capacity functions for the model compound $(Fe)_1(S)_1$ of high-temperature pyrrhotite, FeS (troilite), $Fe_{7.016}S_8$ (monoclinic pyrrhotite), and FeS_2 (pyrite) taken from the SGTE pure substances database and for Fe_9S_{10} obtained by fitting experimental data of Grønvold and Stølen (Ref 79)

Compounds	T range, K	$C_p(T)$, J/(mol · K)
$(Fe)_1(S)_1$	298-420	2437.135 − 9.901929 T + 1.156762 T^2 − 41,123,870 T^{-2}
	420-440	83.0
	440-590	344.055 − 1.1307420 T + 0.1173304E-02 T^2 − 13,870 T^{-2}
	590-1200	36.401 + 0.236417E-01 T − 0.553585E-05 T^2 + 3,740,990 T^{-2}
	1200-1400	47.203 + 0.82851E-02 T + 0.36613E-06 T^2 + 2,482,690.0 T^{-2}
FeS	298-420	2437.135 − 9.9019290 T + 0.11567620E-01 T^2 − 41,123,870 T^{-2}
Fe_9S_{10}	298-495	170.59429 − 0.454379 T + 0.549140579E-3 T^2 − 2,995,243.9 T^{-2}
	495-534	−120,982.043 + 309.185782 T − 0.221712 T^2 + 5.472063E+09
$Fe_{7.016}S_8$	298-600	140.4944 + 0.7210568 T − 3.0600792E-07 T^2 + 3,867,416 T^{-2}
FeS_2	298-1350	72.387 + 8.8501E-03 T + 7.3E-10 T^2 − 1.14279E+06

Note: T, temperature; C_p, heat capacity

Gibbs energy of hypothetical S with $B8_1$ structure. The excess Gibbs energy expression is expanded as a Redlich-Kister polynomial:

$$G^{ex} = y_{Fe}y_{Va}\sum_{n\geq 0} {}^nL_{(Fe,Va:S)}(y_{Fe} - y_{Va})^n \quad \text{(Eq 10)}$$

where the model parameters ${}^nL_{(Fe,Va:S)}$ may be temperature-dependent.

3.5 Stoichiometric Compounds

Phase diagram information in the literature (Ref 1, 3, 4) indicates that six solid phases of the Fe-S system can be interpreted as line compounds: troilite (FeS), $Fe_{11}S_{12}$, $Fe_{10}S_{11}$, Fe_9S_{10}, Fe_7S_8, and pyrite (FeS_2). Consequently, the Gibbs energy functions of these stoichiometric compounds are modeled as depending only on temperature:

$$G = \Delta_f H_{298} + \int_{298.15}^{T} C_p dT - T\left[S_{298} + \int_{298.15}^{T} (C_p/T)dT\right] \quad \text{(Eq 11)}$$

This equation contains the standard enthalpy of formation $\Delta_f H_{298}$ and the standard entropy S_{298} at 298.15 K, and the heat capacity at constant pressure C_p, which is a function of temperature.

Table 6 Comparison of the calculated invariant equilibria with experimental (Ref 4, 31) and assessed values (Ref 1, 3, 20, 34)

Invariant equilibrium	*T*, °C	Composition, at.% S			Reference
bcc-(Fe)/liquid	1538	0.0	0.0	…	1
	1538	0.0	0.0	…	calc
fcc-(Fe)/bcc-(Fe)	1394	0.0	0.0	…	1
	1394	0.0	0.0	…	calc
fcc-(Fe)/bcc-(Fe)/liquid	1365 ± 10	0.090	0.24	~20.0	1
	1356.4	0.085	0.22	21.2	calc
fcc-(Fe)/liquid/$Fe_{1-x}S$	988	~0.018	44.6	50.0	1
	988	0.019	43.6	50.1	calc
fcc-(Fe)/bcc-(Fe)/$Fe_{1-x}S$	927	~0.006	0.033	50.0	1
	914	0.010	0.032	50.0	calc
fcc-(Fe)/bcc-(Fe)	912	0.0	0.0	…	1
	912	0.0	0.0	…	calc
$Fe_{1-x}S$/liquid	1188	~52.0	~52.0	…	1
	1189	51.9	51.9	…	calc
$Fe_{1-x}S$/liquid(1)/liquid(2)	1082 ± 3	54.2	~64.5	~99.7	1
	1092 ± 3	54.6 ± 0.5	64.4 ± 1.9	99.7	31
	1091	54.7	64.5	99.6	calc
$Fe_{1-x}S/FeS_2$/liquid	743	55.0	~66.67	~99.94	1
	743	55.8	66.67	99.98	calc
Liquid/monoclinic-S	115.22	100.0	100.0	…	1
	115.21	100.0	100.0	…	calc
Monoclinic-S/orthorhombic-S	95.15	100.0	100.0	…	20, 34
	95.15	100.0	100.0	…	calc
FeS_2/liquid/monoclinic-S	115.21	66.67	100.0	100.0	calc
FeS_2/monoclinic-S/orthorhombic-S	95.15	66.67	100.0	100.0	calc
$Fe_{1-x}S/Fe_{7.016}S_8/FeS_2$	317.85	52.63	53.27	66.67	3
	316.9	52.65	53.28	66.67	calc
$Fe_{1-x}S/Fe_9S_{10}/Fe_{7.016}S_8$	261.8	52.47	52.63	53.19	3
	260.2	52.06	52.63	53.28	calc
$Fe_{1-x}S/Fe_{10}S_{11}/Fe_9S_{10}$	183.9	51.46	52.38	52.63	calc
$Fe_{1-x}S/Fe_{11}S_{12}/Fe_{10}S_{11}$	131.0	51.16	52.17	52.38	calc
$FeS/Fe_{1-x}S/Fe_{11}S_{12}$	100.0	50.00	51.43	?	4
	95.5	50.00	51.01	52.17	calc
bcc-(Fe)/FeS/$Fe_{1-x}S$	146.45	0.00	50.00	50.03	3
	146.6	0.00	50.00	50.01	calc

Note: *T*, temperature; calc, calculated

4. Results

The calculations of thermodynamic properties and phase diagrams were carried out with the thermodynamic software package FactSage (Ref 73); the optimization computations were performed with the software ChemSage (Ref 74) and its routine for parameter optimization (Ref 75). Standard Gibbs energy functions, G_i^0, for pure Fe and S in the gaseous, liquid, and solid states were taken from the Scientific Group Thermodata Europe (SGTE) unary database for pure elements, compiled by Dinsdale (Ref 76) for the condensed states. These data are consistent with all observed phase-transformation temperatures.

The selected standard Gibbs energy function of pure liquid S takes into account the occurrence of a λ-transition at 432 K and is also used for estimating the Gibbs energy of supercritical S. For the gas phase, standard Gibbs energy functions for $S_n(g)$ from $S_1(g)$ to $S_8(g)$ as well as Fe(g) and FeS(g) are taken into consideration. The chosen standard Gibbs energy function for pure αFe includes energetic contributions due to ferromagnetism.

4.1 Optimized Model Quantities

Tables 1 through 4 present all optimized model parameters in this work. As they originate from computations, at least two digits are given after the decimal point for enthalpies and entropies to enable the reader to reproduce precisely all the data presented in the tables and figures of this article. In Table 5, all heat-capacity temperature functions related to model compounds as well as to the stoichiometric phases treated in this work are listed.

Table 1 gives the optimized excess Gibbs energy param-

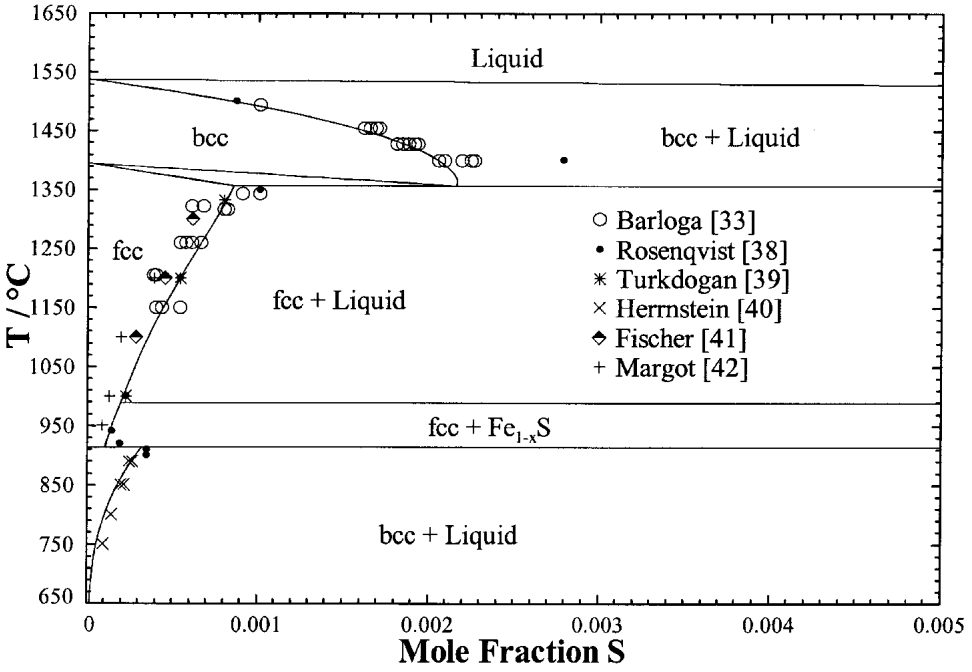

Fig. 2 Calculated, optimized partial Fe-S phase diagram together with experimental data

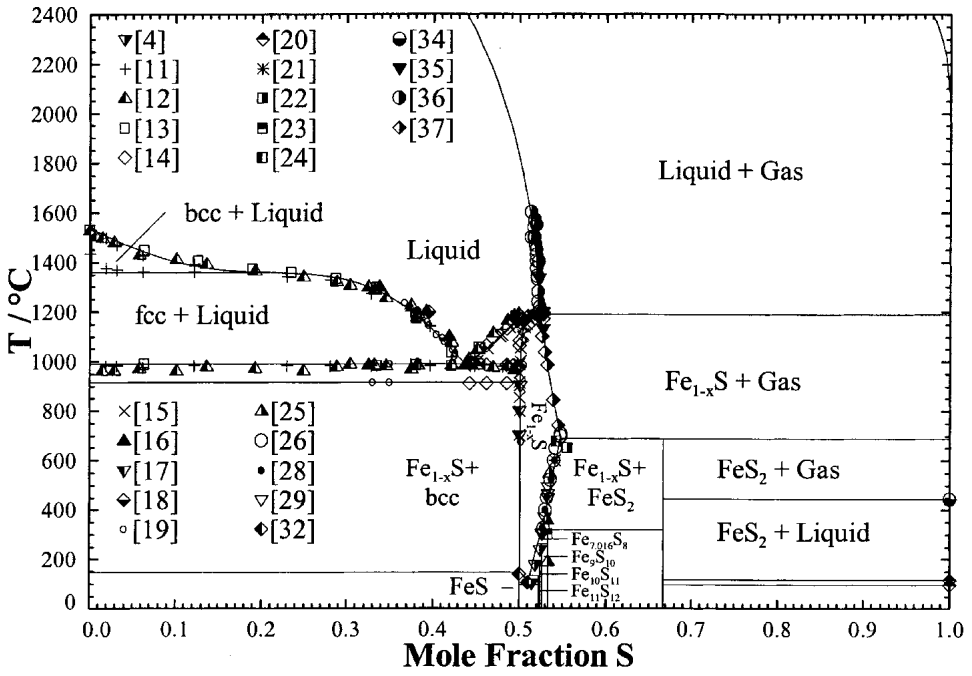

Fig. 3 Calculated, optimized Fe-S phase diagram at a total pressure of 1 bar together with experimental data

eters of Eq 4 for the liquid phase. Because the composition of maximum short-range ordering is at 50 mol% S, the binary coordination numbers Z_{FeS} and Z_{SFe} are set equal to each other. It was found that a value of 2 for the binary coordination numbers Z_{FeS} and Z_{Sfe} and a value of 6 for the unary coordination numbers Z_{SS} and Z_{FeFe}, give the best optimization results. The "nonphysical" character of the coordination numbers results from the *mathematical* approximation of using the one-dimensional Ising expression for the configurational entropy (the three-dimensional Ising expression being mathematically intractable) (Ref 66).

The Gibbs energy expression of Eq 7, which was chosen for the Fe solid solutions (α- and δFe with bcc structure, γFe with fcc structure) requires standard Gibbs energies for

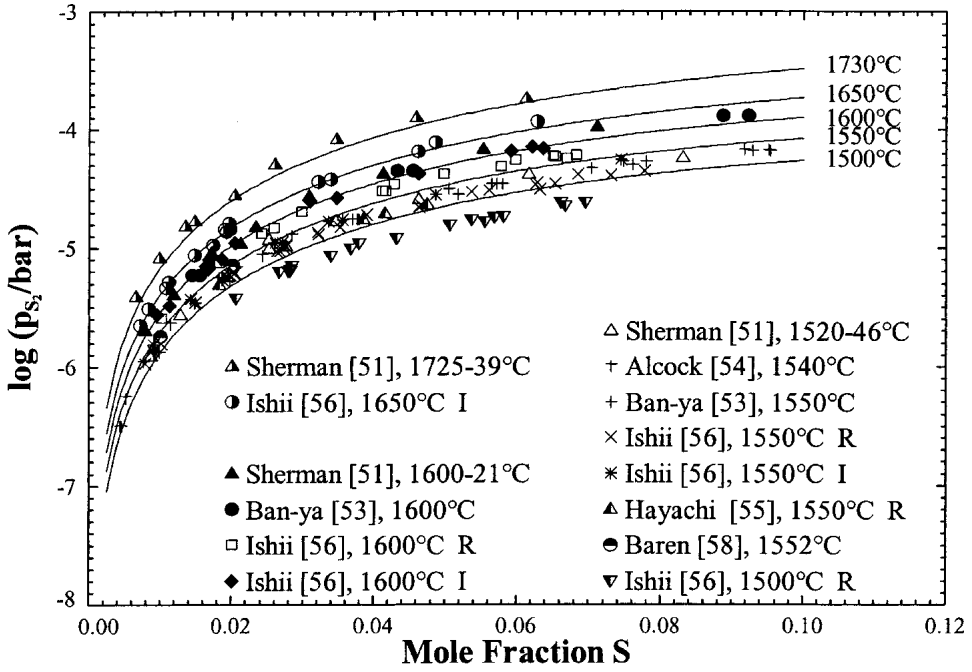

Fig. 4 Calculated S potential of the liquid phase up to S mole fractions of 0.1 together with experimental data. I, induction furnace; R, resistance furnace

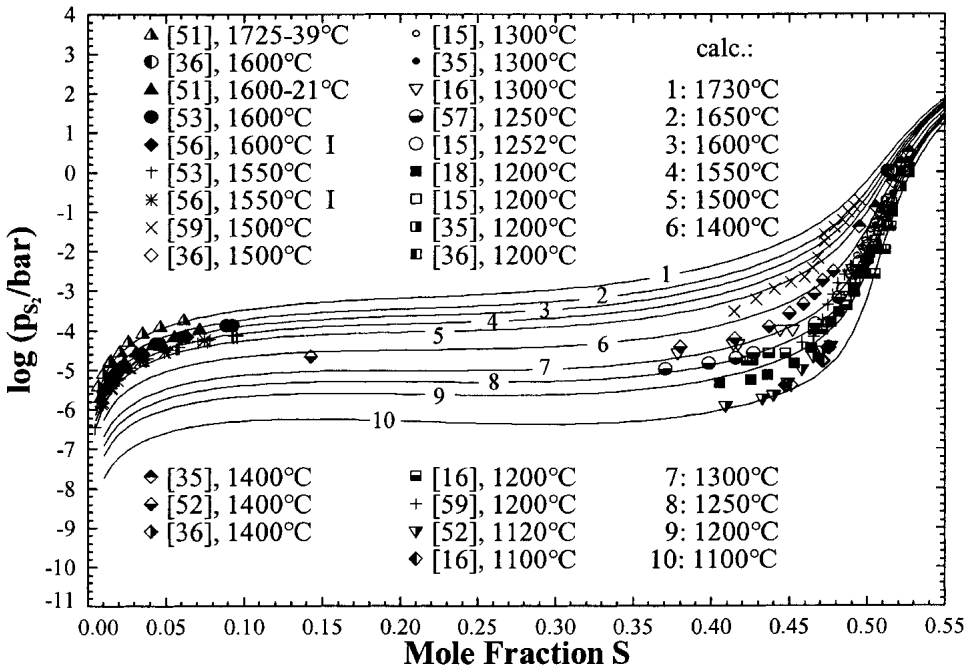

Fig. 5 Calculated S potential of the liquid phase up to S mole fractions of 0.55 together with experimental data. I, induction furnace

hypothetical pure solid S with the bcc and fcc structures. These model parameters are chosen so that these allotropes are less stable than pure monoclinic, orthorhombic, liquid, and gaseous S. The heat capacities for both structures were estimated as being equal to the heat capacity of orthorhombic S (Ref 76). The optimized enthalpies of formation at 298.15 K for bcc- and fcc-S relative to elemental S in its most stable state at 298.15 K were calculated to be 24,954.78 and 66,082.63 J/mol, respectively. For the absolute third-law entropies at 298.15 K, optimized values of 46.377 and 22.444 J/(mol · K) were obtained. In addition, one optimized temperature-dependent interaction parameter for each phase, as defined by Eq 8, was obtained. All optimized parameters are presented in Table 2.

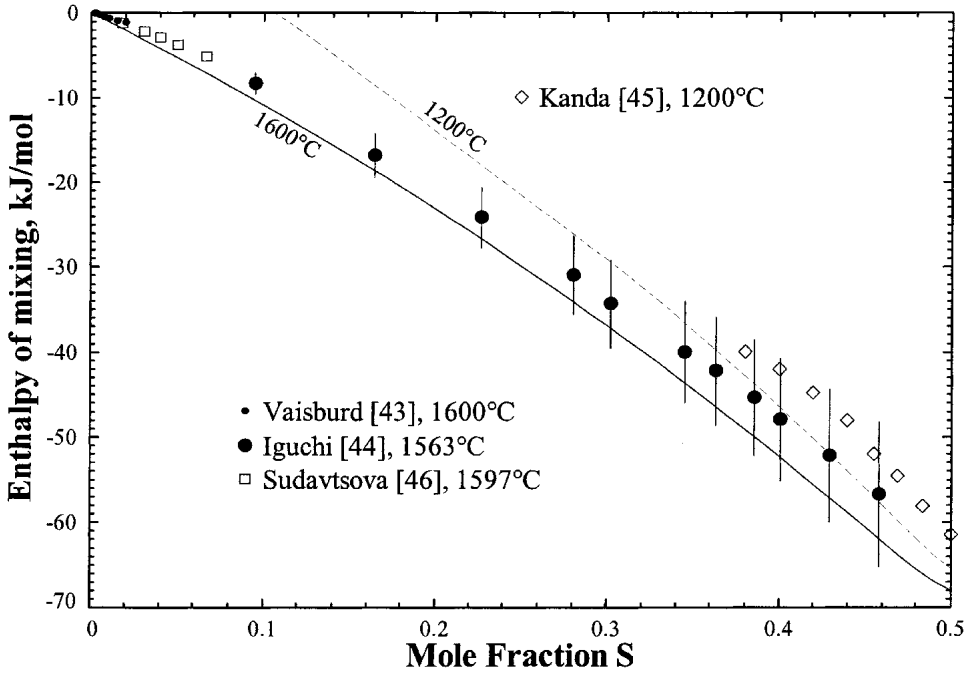

Fig. 6 Calculated enthalpy of mixing of 0.5 S_2(gas) and either fcc-(Fe) at 1200 °C or liquid Fe at other temperatures shown to give liquid mixtures at the same temperature, together with experimental data

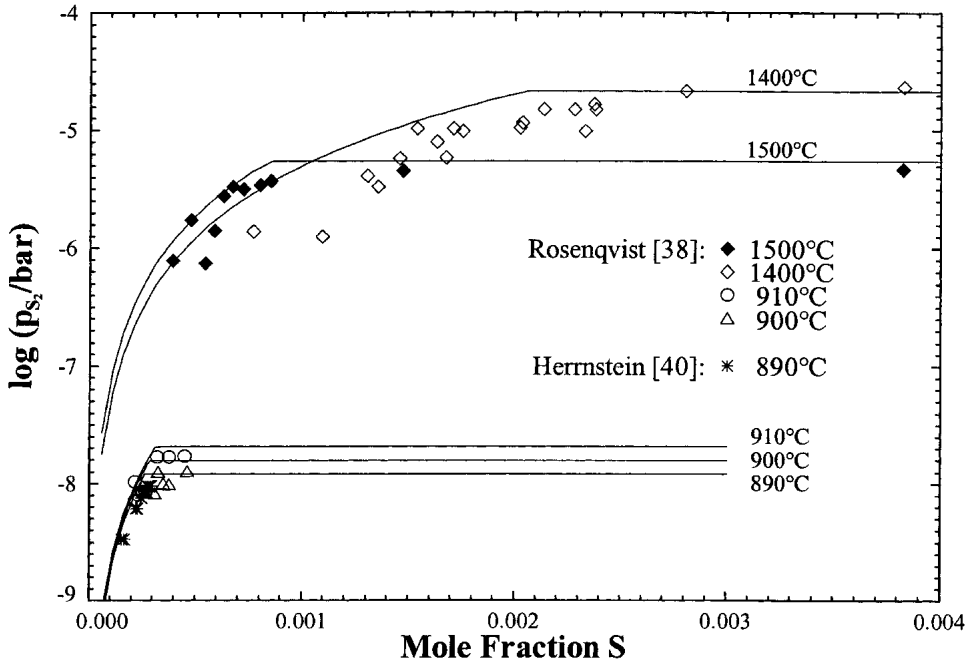

Fig. 7 Calculated S potential of bcc Fe solid solution and adjacent two-phase regions, together with experimental data

According to the sublattice model for the Gibbs energy of high-temperature pyrrhotite, two "compounds," $(Fe)_1(S)_1$ and $(Va)_1(S)_1$, occur in Eq 9. The heat-capacity function of $(Fe)_1(S)_1$, which is listed in Table 5, is taken, along with a transition enthalpy of 290 J/mol at 590 K, from the SGTE pure substances database for stoichiometric FeS, which reproduces the most recent experimental data of Grønvold and Stølen (Ref 3). The heat capacity of $(Va)_1(S)_1$ and its absolute third-law entropy at 298.15 K were estimated as being equal to the corresponding quantities of pure orthorhombic S (Ref 76). In Table 3, all optimized model parameters defined by Eq 9 and 10 are given. These are the enthalpies of formation for both sublattice compounds at 298.15 K relative to the elements in their most stable states

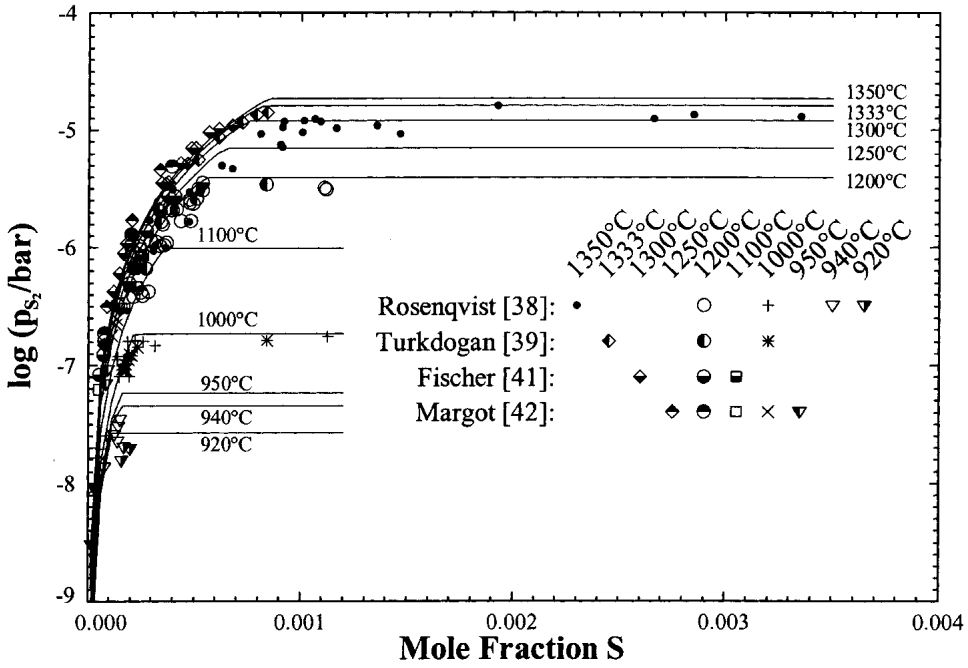

Fig. 8 Calculated S potential of fcc Fe solid solution and adjacent two-phase regions, together with experimental data

at 298.15 K, and the entropy of $(Fe)_1(S)_1$ at 298.15 K, as well as one temperature-dependent interaction parameter.

Six solid phases [FeS (troilite), $Fe_{11}S_{12}$, $Fe_{10}S_{11}$, Fe_9S_{10}, $Fe_{7.016}S_8$ (monoclinic pyrrhotite), and FeS_2 (pyrite)] were taken into consideration as stoichiometric compounds in this work. The stoichiometry of monoclinic pyrrhotite, $Fe_{7.016}S_8$, was chosen to represent the small homogeneity range around the composition Fe_7S_8, which has, up to now, been only quantitatively reported in the literature. Data from the literature (Ref 3, 34, 77-79) served as starting values in the optimization of the enthalpies of formation and entropies at 298.15 K of troilite, Fe_9S_{10}, $Fe_{7.016}S_8$, and pyrite, and then were adjusted within the experimental error limits in the optimization process. Table 5 shows the heat-capacity functions, $C_p(T)$, that were used. For FeS (troilite) and $Fe_{7.016}S_8$ (monoclinic pyrrhotite), these functions describe the most recent experimental data of Grønvold and Stølen (Ref 3). For FeS_2 (pyrite), the function is accepted from the SGTE pure substances database. The heat-capacity function of Fe_9S_{10} in Table 5 was obtained by fitting the recent experimental data of Grønvold et al. (Ref 79). In addition, a transition enthalpy of 119.72 J/mol at 495 K is taken from Grønvold et al. (Ref 79). Thermodynamic data for the compounds $Fe_{11}S_{12}$ and $Fe_{10}S_{11}$ are completely lacking in the literature. Consequently, their heat-capacity functions were estimated from the heat-capacity function of $Fe_{7.016}S_8$ by weighting with the corresponding stoichiometric factors (e.g., the C_p of $Fe_{11}S_{12}$ = 23/15.016 × C_p of $Fe_{7.016}S_8$).

Table 4 gives the optimized parameters of Eq 11. These are the enthalpies of formation relative to the elements in their most stable states at 298.15 K and the absolute third-law entropies at 298.15 K of all six solid phases treated as line compounds in this work. All values are within error limits given in the literature (Ref 34, 77, 78), except for $Fe_{11}S_{12}$ and $Fe_{10}S_{11}$, for which no data could be found in the literature.

4.2 Comparison of Calculations and Experimental Data

In Fig. 1, the complete condensed, calculated phase diagram is shown along with experimental data (Ref 4, 11-32). It can be seen that all experimental phase boundary data for equilibria involving the liquid phase, fcc-(Fe), bcc-(Fe), $Fe_{1-x}S$, troilite FeS through $Fe_{11}S_{12}$, $Fe_{10}S_{11}$, Fe_9S_{10} to monoclinic pyrrhotite $Fe_{7.016}S_8$, pyrite FeS_2, and finally monoclinic and orthorhombic S are reproduced very satisfactorily. Table 6 gives a compilation of all calculated invariant equilibria together with the experimental values (Ref 4, 31) and assessed values (Ref 1, 3, 20, 34) of invariant temperatures and compositions of the phases involved. The Gibbs energy model for phases of the pyrrhotite group can be seen to give satisfactory agreement with the phase diagram data from the literature (Ref 3, 4). Due to the lack of experimental information about the precise phase relations among $Fe_{11}S_{12}$, $Fe_{10}S_{11}$, and Fe_9S_{10} in the region of the pyrrhotite group, the present modeling resulting in a cascade of peritectoid equilibria between 90 and 320 °C was accepted. Figure 2 shows details of the calculated phase diagram involving Fe-rich alloys. It can be seen that all available S solubility data (Ref 33, 38-42) for bcc-(Fe) and fcc-(Fe) are reproduced within the experimental scatter.

In this work, the pressure dependencies of the Gibbs energies of the condensed phases were neglected. However, pressures up to several hundred bars are expected to have only a small influence on the Gibbs energy functions of the solid phases and the melt. Figure 3 shows the calculated phase diagram at 1 bar total pressure together with experimental data (Ref 4, 11-26, 28, 29, 32, 34-37). The stability

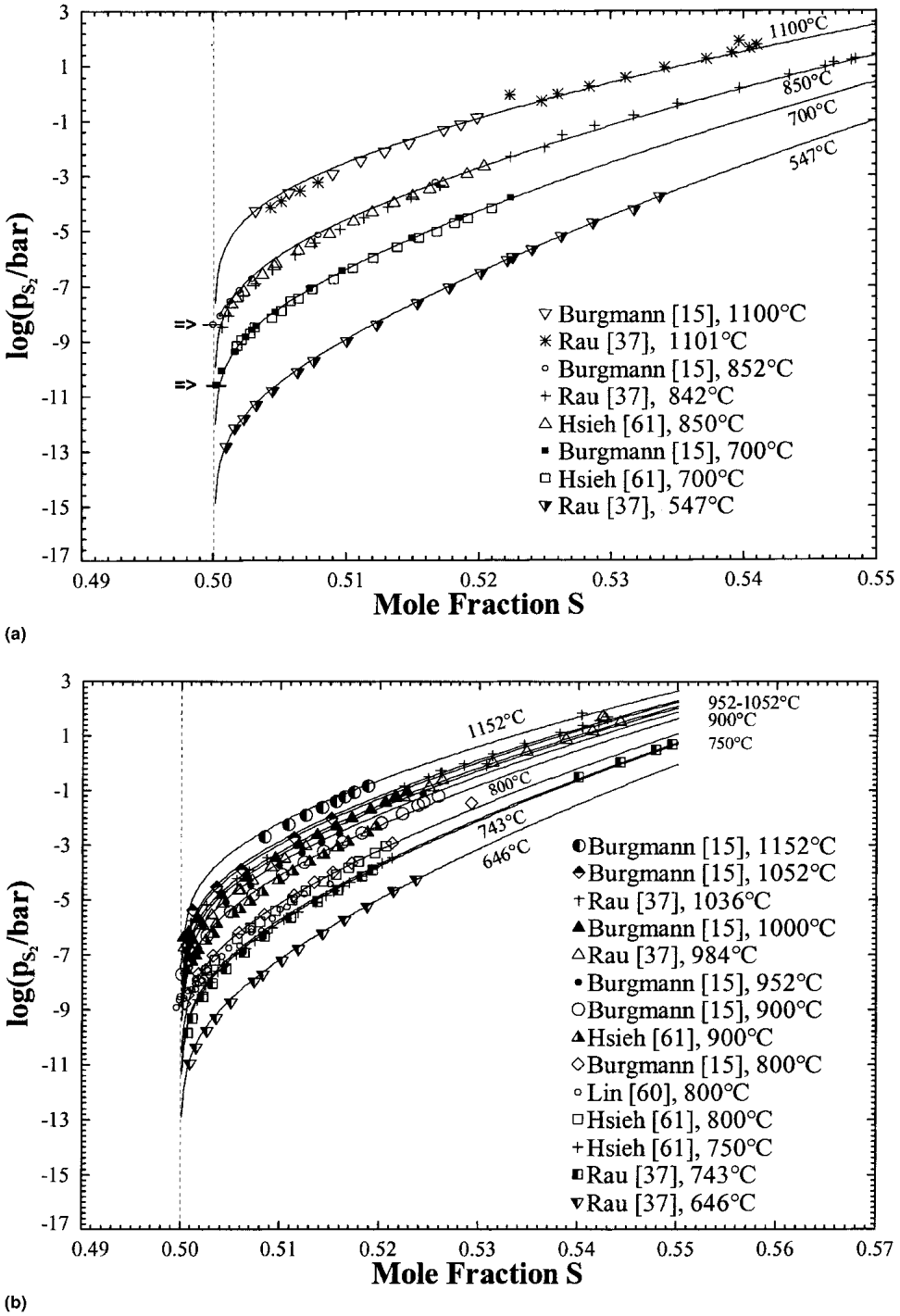

Fig. 9 (a) Calculated S potential of $Fe_{1-x}S$ together with experimental data. For two data points, depicted by two arrows (=>), error bars are shown (see text for detailed discussion). (b) Calculated S potential of $Fe_{1-x}S$ together with experimental data

fields involving the gas phase replace the miscibility gap (experimentally observed at the monotectic three-phase invariant) between a sulfide melt and an almost pure S liquid phase (in a strict sense, "fluid," if the critical pressure of S is exceeded). It can be seen that the present work also permits a satisfactory computation of liquid/gas as well as $Fe_{1-x}S$/gas equilibria at 1 bar total pressure.

Figure 4 compares calculated and experimental S potentials in Fe-rich melts (Ref 51, 53-56, 58). Figure 5 gives an overview of the calculated and experimental S potentials for the ranges of temperature (from 1100-1740 °C) and composition (up to 53 mol% S) over which the experimental measurements have been reported (Ref 15, 16, 18, 35, 36, 51-53, 56, 57, 59). For the sake of clarity, not all of the data

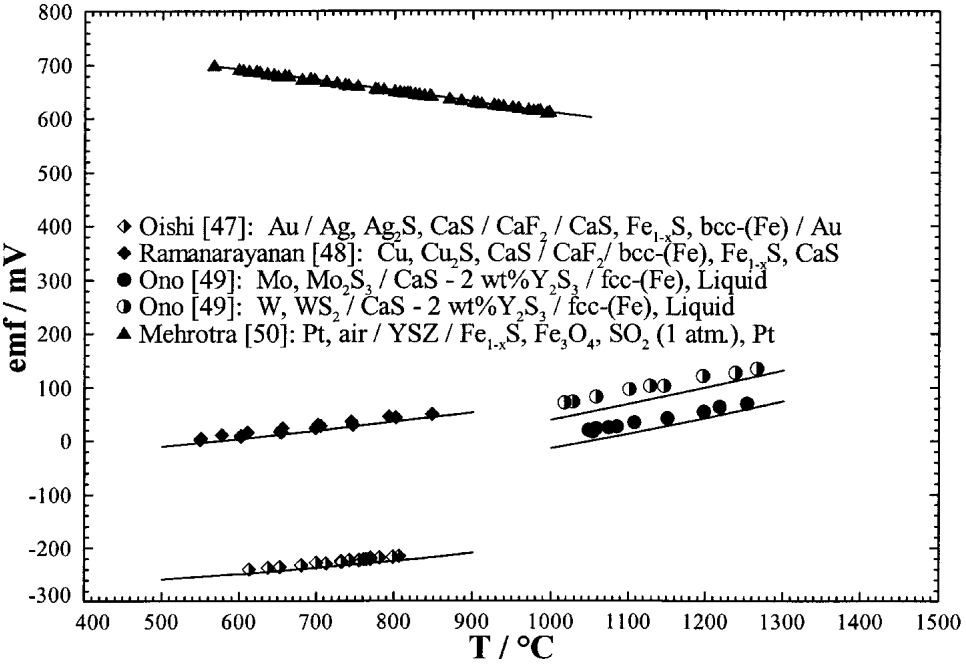

Fig. 10 Calculated emf together with experimental data for various electrochemical cells

for Fe-rich solutions given in Fig. 4 are shown in Fig. 5. Agreement of the calculations with the experimental data is good to very good.

In addition, as shown in Fig. 6, the model for the liquid phase also permits the calculation of the enthalpy of mixing at near 1200 and 1600 °C within the error limits of the experimental data (Ref 43-46).

Figures 7 and 8 demonstrate a satisfying agreement of S potentials (Ref 38-42) measured for bcc-(Fe) at temperatures from 890 through 1500 °C and for fcc-(Fe) at temperatures from 920 through 1350 °C with the calculations. Agreement is also good in the adjacent two-phase regions.

The optimized model parameters of the two-sublattice model for $Fe_{1-x}S$ allow correct reproduction of the experimental S potentials (Ref 15, 37, 60, 61) over a wide temperature range from about 550 to 1150 °C, as demonstrated in Fig. 9(a) and (b). Only the data points given by Burgmann et al. (Ref 15) at 700, 842, and 1100 °C in Fig. 9(a) were used to obtain the optimized parameters. The other data points in Fig. 9(a) and all points in Fig. 9(b) were predicted very satisfactorily. Consequently, the model for pyrrhotite, $Fe_{1-x}S$, provides a quantitative relationship among temperature, metal deficiency, and S partial pressure over the whole homogeneity range of the phase. Although additional experimental information about the S activities of pyrrhotite is available in the literature, only data from selected experimental articles are shown in Fig. 9(a) and (b). It should be mentioned that these articles are the same as those selected by Chuang et al. (Ref 9) in their study. This enables a direct comparison to be made between the model description used in the present work and the model of Chuang et al. (Ref 9), which assumed the presence of Fe on interstitial sites. For two data points, which are indicated by two arrows in Fig. 9(a), experimental error bars are drawn to show the uncertainty of the experimental evidence for a possible deviation of pyrrhotite to the Fe-rich side of stoichiometric FeS, as was assumed by Chuang et al. (Ref 9) and Rau (Ref 37). In fact, as shown in Fig. 9(b), there is only one article (Ref 60) in which some data points were reported at S mole fractions of <0.5. Unfortunately, no error ranges were given (Ref 60). Assuming the same uncertainty as shown by the error bars in Fig. 9(a), the experimental evidence does not seem sufficient to justify a more complex model involving a possible small S-deficient homogeneity range.

Figure 10 shows the experimental results of emf studies (Ref 47-49) with various types of electrochemical cells in which the first two studies (Ref 47, 48) and the final study (Ref 49) are related to the two-phase equilibria bcc-(Fe)/$Fe_{1-x}S$ and fcc-(Fe)/liquid, respectively. The present model was used to simulate these emf measurements. Agreement between calculations and experiments ranged from fair to good. For the monophase region of $Fe_{1-x}S$, agreement with the experimental results of Mehrotra and Wagner (Ref 50) was very good.

Finally, Fig. 11 presents the calculated log (p_{S_2}/bar)-1/T diagram. Agreement with numerous experimental data points for two- and three-phase equilibria (Ref 15-18, 24, 29, 38, 40-42, 57, 62-65) was very satisfactory.

5. Discussion

In a recent article (Ref 80), the authors reported on a similar optimization of the entire Ni-S system. Based on this, on the present optimization of the Fe-S system, and on an optimization of the Fe-Ni system, the authors have recently performed an evaluation/optimization of the com-

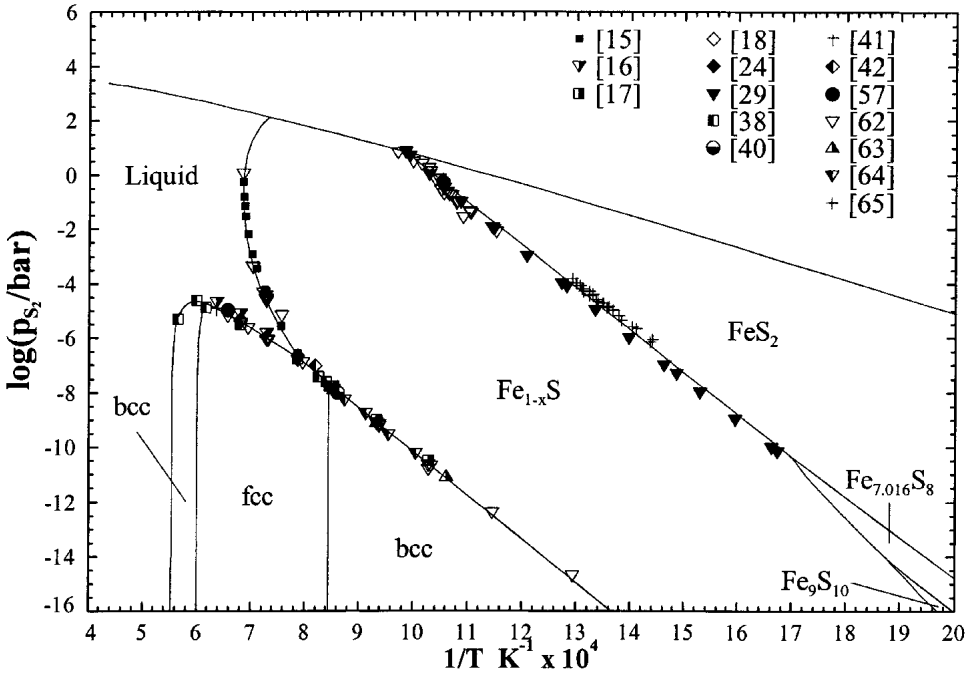

Fig. 11 Calculated $\log(p_{S_2}/\text{bar})$-$1/T$ diagram together with experimental data

plete ternary Fe-Ni-S system, which has been reported elsewhere (Ref 81). It was shown (Ref 81) that a complete thermodynamic description of the ternary liquid phase is provided by the modified quasi-chemical model with only three additional ternary parameters. Even with no additional ternary parameters, a reasonable description of the properties of the ternary liquid was obtained based solely on the binary parameters.

6. Conclusions

The Gibbs energies of ten binary Fe-S phases have been modeled, and optimized model parameters have been obtained, thereby providing a satisfactory and thermodynamically consistent simultaneous description of a large amount of phase equilibria and thermodynamic data. Recent extensions of the modified quasi-chemical model have been successfully applied for the first time to a metal-S liquid phase. Gibbs energy modeling of low-temperature phases in the region of the pyrrhotite group has been carried out within the framework of a complete thermodynamic study of the binary Fe-S system. The present assessment can be used as a key subsystem in the development of thermodynamic databases for multicomponent metal-S systems.

Acknowledgments

This project was supported by a Collaborative Research and Development (CRD) grant from the Natural Sciences and Engineering Research Council of Canada in collaboration with INCO, Noranda, Rio Tinto, Teck Cominco, Alcoa, Dupont, Shell, Corning, Pechiney, Norsk Hydro, Sintef, Schott Glas, St.-Gobain Recherche, Mentek, and IIS Materials. One of the authors (P.W.) wishes to thank the Austrian Science Foundation for financial assistance.

References

1. O. Kubaschewski, *Phase Diagrams of Binary Iron Alloys,* H. Okamoto, Ed., ASM International, 1993, p 364-366
2. F. Power and H.A. Fine, The Iron-Sulphur System, *Miner. Sci. Eng.,* Vol 8, 1976, p 106-128
3. F. Grønvold and S. Stølen, Thermodynamics of Iron Sulfides II. Heat Capacity and Thermodynamic Properties of FeS and $Fe_{0.875}S$ at Temperatures from 298.15 K to 1000 K, of $Fe_{0.98}S$ from 298.15 K to 800 K, and $Fe_{0.89}S$ from 298.15 K to about 650 K: Thermodynamics of Formation, *J. Chem. Thermodyn.,* Vol 24, 1992, p 913-936
4. H. Nakazawa and N. Morimoto, Phase Relations and Superstructures of Pyrrhotite, $Fe_{1-x}S$, *Mater. Res. Bull.,* Vol 6, 1971, p 345-358
5. M. Hillert and L.-I. Staffansson, An Analysis of the Phase Equilibria in the Fe-FeS System, *Metall. Trans. B,* Vol 6, 1975, p 37-41
6. R.C. Sharma and Y.A. Chang, Thermodynamics and Phase Relationships of Transition Metal-Sulfur Systems: Part III. Thermodynamic Properties of the Fe-S Liquid Phase and the Calculation of the Fe-S Phase Diagram, *Metall. Trans. B,* Vol 10, 1979, p 103-108
7. G.G. Libowitz, Energetics of Defect Formation and Interaction in Nonstoichiometric Pyrrhotite, *Reactivity of Solids, Proc. 7th Int. Symp.,* J.B. Anderson, M.W. Robertson, and P.S. Stone, ed., Chapman and Hall, London, 1972, p 107-115
8. A.F. Guillermet, M. Hillert, B. Jansson, and B. Sundman, An Assessment of the Fe-S System Using a Two-Sublattice Model for the Liquid Phase, *Metall. Trans. B,* Vol 12, 1981, p 745-754

9. Y.-Y. Chuang, K.-C. Hsieh, and Y.A. Chang, Thermodynamics and Phase Relationships of Transition Metal-Sulfur Systems, Part V: A Re-evaluation of the Fe-S System Using an Associated Solution Model for the Liquid Phase, *Metall. Trans. B,* Vol 16, 1985, p 277-285
10. F. Kongoli, Y. Dessureault, and A.D. Pelton, Thermodynamic Modeling of Liquid Fe-Ni-Cu-Co-S Mattes, *Metall. Mater. Trans. B,* Vol 29, 1998, p 591-601
11. K. Friedrich, Note on the Melting Diagram of the System FeS-Fe, *Metallurgie,* Vol 7, 1910, p 257-261 (in German)
12. R. Loebe and E. Becker, The System Iron-Iron Sulfide, *Z. Anorg. Chem.,* Vol 77, 1912, p 301-319 (in German)
13. K. Miyazaki, The Equilibrium Diagram of the Iron and Iron Sulphide System, *Sci. Rep. Tohoku Imp. Univ., Ser. 1,* Vol 17, 1928, p 877-882
14. E. Jensen, Pyrrhotite: Melting Relations and Composition, *Am. J. Sci.,* Vol 240, 1942, p 695-699
15. W. Burgmann, G. Urbain, and M.G. Frohberg, Contribution to the Study of the System Fe-S in the Region of Iron Sulfide (Pyrrhotite), *Mem. Sci. Rev. Met.,* Vol 65, 1968, p 567-578 (in French)
16. M. Nagamori, T. Hatakeyama, and M. Kameda, Thermodynamics of Fe-S Melts between 1100 and 1300°C, *Trans. JIM,* Vol 11, 1970, p 190-194
17. M. Nagamori, Technical Note: Compositions and Free Energies of Ag_2S and FeS Saturated with Metal, *Can. Metall. Q.,* Vol 9, 1970, p 531-533
18. C.W. Bale and J.M. Toguri, Thermodynamics of the Cu-S, Fe-S and Cu-Fe-S Systems, *Can. Metall. Q.,* Vol 15, 1976, p 305-318
19. Y.-Y. Chuang, "The Thermodynamics and Phase Relationships of the Cu-Ni-Fe-S Quaternary System and Its Subsystems," Ph.D. dissertation, University of Wisconsin-Madison, 1983
20. L.V. Gurvic, I.V. Veyts, and C.B. Alcock, *Thermodynamic Properties of Individual Properties,* 4th ed., Hemisphere Publishing Co., 1989, p 265-316
21. E.T. Allen, J.L. Crenshaw, and J. Johnston, Iron-Sulfur Minerals, *Z. Anorg. Chem.,* Vol 76, 1912, p 201-273
22. G. Hägg and I. Sucksdorff, The Crystal Structure of Troilite and Pyrrhotite, *Z. Phys. Chem. B,* Vol 22, 1933, p 444-452 (in German)
23. H.S. Roberts, Polymorphism in the FeS-S Solid Solutions, I: Thermal Study, *J. Am. Chem. Soc.,* Vol 57, 1935, p 1034-1038
24. H.E. Merwin and R.H. Lombard, The System Cu-Fe-S, *Econ. Geol.,* Vol 32, 1937, p 203-284
25. F. Grønvold and H. Haraldsen, On the Phase Relations of Synthetic and Natural Pyrrhotites ($Fe_{1-x}S$), *Acta Chem. Scand.,* Vol 6, 1952, p 1452-1469
26. R.G. Arnold, "Pyrrhotite-Pyrite Equilibrium Relations between 325° and 743°C," PhD dissertation, Princeton University, 1958
27. G. Kullerud, Two-Liquid Field in the Fe-S System, *Carnegie Inst. Washington Yearbk.,* Vol 60, 1961, p 174-176
28. R.G. Arnold, Equilibrium Relations between Pyrrhotite and Pyrite from 325 to 743 °C, *Econ. Geol.,* Vol 57, 1962, p 72-90
29. P. Toulmin and P.B. Barton, A Thermodynamic Study of Pyrite and Pyrrhotite, *Geochim. Cosmochim. Acta,* Vol 28, 1964, p 641-671
30. G. Kullerud and H.S. Yoder, Pyrite Stability Relations in the Fe-S System, *Econ. Geol.,* Vol 54, 1959, p 533-572
31. R.G. Arnold, Evidence for Liquid Immiscibility in the System FeS-S, *Econ. Geol.,* Vol 66, 1971, p 1121-1130
32. G.H. Moh and G. Kullerud, Phase Relations at Low Temperatures: The Fe-S System, *Carnegie Inst. Washington Yearbk.,* Vol 63, 1964, p 207-208
33. A.M. Barloga, K.R. Bock, and N. Parlee, The Iron-Carbon-Sulfur System from 1149° to 1427°C, *Trans. AIME,* Vol 221, 1961, p 173-179
34. M.W. Chase Jr., C.A. Davies, J.R. Downey, Jr., D.J. Frurip, R.A. McDonald, and A.N. Syverud, JANAF Thermochemical Tables, 3rd ed., *J. Phys. Chem. Ref. Data,* Vol 14 (Suppl. 1), 1985, p 1774-1777
35. A.V. Ditman and I.N. Vechko, Dissociation of Iron Sulfide at High Temperatures, Measured by the Dew Point Method, *Inorg. Mater.,* Vol 1, 1965, p 1394-1399
36. E. Schürmann and H.J. Henke, Investigation of the Sulfur Equilibrium Pressure in the Binary System Iron-Sulfur at 1200-1600°C at Atmospheric Pressure, *Giessereiforsch.,* Vol 23, 1971, p 165-168 (in German)
37. H. Rau, Energetics of Defect Formation and Interaction in Pyrrhotite $Fe_{1-x}S$ and Its Homogeneity Range, *J. Phys. Chem. Solids,* Vol 37, 1976, p 425-429
38. T. Rosenqvist and B.L. Dunicz, Solid Solubility of Sulphur in Iron, *Trans. AIME,* Vol 194, 1952, p 604-608
39. E.T. Turkdogan, S. Ignatowicz, and J. Pearson, The Solubility of Sulphur in Iron and Iron-Manganese Alloys, *J. Iron Steel Inst.,* Vol 180, 1955, p 349-354
40. W.H. Herrnstein, F.H. Beck, and M.G. Fontana, Solubility and Permeability of Sulfur in Alpha Iron," *Trans. AIME,* Vol 242, 1968, p 1049-1056
41. M. Fischer and K. Schwerdtfeger, Thermodynamics of the System Fe-Mn-S: Part II. Solubility of Sulfur and Manganese in γ-Iron Coexisting with Sulfide in the Temperature Range 1100 to 1300°C, *Metall. Trans. B,* Vol 9, 1978, p 631-634
42. E. Margot, B. Venard, N. Barbouth, and J. Oudar, Study of the Solubility of Sulfur in γ-Iron, *C.R. Acad. Sci.,* Vol 272, 1971, p 373-376 (in French)
43. S.E. Vaisburd, V.G. Dyubanov, A.Ya. Stomakhin, I.N. Zedina, and A.F. Filippov, Enthalpies of Sulfur Dissolution in Fe and Ni, *Chern. Metall.,* 1972, p 53-55 (in Russian)
44. Y. Iguchi, Y. Tozaki, and M. Kakizaki, A Calorimetric Study of Heats of Mixing of Liquid Iron Alloys, *Tetsu to Hagane,* Vol 67, 1981, p 925-932 (in Japanese)
45. M. Kanda, N. Hasegawa, K. Itagaki, and A. Yazawa, Thermodynamic Study of the Liquid Fe-S System by Use of a Drop Calorimeter, *Thermochim. Acta,* Vol 109, 1986, p 275-284
46. V.S. Sudavtsova, N.O. Sharkina, and V.G. Kudin, The Thermodynamic Properties of Liquid Melts in the Fe-S and Fe-S-Metal Systems, *Russ. J. Phys. Chem. (Engl. Trans.),* Vol 75, 2001, p 1061-1064
47. T. Oishi, T. Fujimura, K. Ogura, and J. Moriyama, Thermodynamic Studies of MnS and FeS by CaF_2 Solid Electrolyte Galvanic Cell, *Nippon Kinzoku Gakkaishi,* Vol 40, 1976, p 969-973 (in Japanese)
48. T.A. Ramanarayanan and W.L. Worrell, The Measurement of Sulfur Chemical Potential Differences Using a CaF_2 Solid Electrolyte, *J. Electrochem. Soc.,* Vol 127, 1980, p 1717-1721
49. K. Ono and J. Moriyama, Galvanic Cells Involving Solid Sulphide Electrolytes for the Determination of Sulphur Chemical Potentials at Elevated Temperatures, *Electrochim. Acta,* Vol 26, 1981, p 1643-1646
50. G.M. Mehrotra and J.B. Wagner, On the Thermodynamic Properties of $Fe_{1-x}S$, *Proc. Electrochem. Soc.,* Vol 86, 1986, p 150-151
51. C.W. Sherman, H.I. Elvander, and J. Chipman, Sulphur in Molten Fe-S Alloys, *AIME,* Vol 188, 1950, p 334-340
52. S. Bog and T. Rosenqvist, *Thermodynamics of Metal Sulfides: IA Thermodynamic Study of the Iron Sulfide-Iron Oxide Melts,*

Royal Norwegian Council of Science and Industrial Research, Trondheim Norges Tekniske-Naturvitens Kapelige Forskiningsrad Metallurgisk Komite, Tech University, Trondheim, Norway, Meddelse No. 12, 1958, p 1-20
53. S. Ban-ya and J. Chipman, Sulfur in Liquid Iron Alloys, Part I: Binary Iron-Sulfur, *Trans. AIME,* Vol 242, 1968, p 940-946
54. C.B. Alcock and L.L. Cheng, A Thermodynamic Study of Dilute Solutions of Sulphur in Liquid Iron, Cobalt and Nickel, and Binary Alloys between these Metals, *J. Iron Steel Inst.,* Vol 195, 1960, p 169-173
55. S. Hayashi and T. Uno, The Activity of S in Liquid Fe, *Nagoya Kogyo Daigaku Gakuho,* Vol 33, 1981, p 261-268 (in Japanese)
56. F. Ishii and T. Fuwa, Activity of Sulfur in Liquid Iron, *Tetsu to Hagane,* Vol 67, 1981, p 736-745 (in Japanese)
57. J. Koh and A. Yazawa, Thermodynamic Properties of the Cu-S, Fe-S and Cu-Fe-S Systems, *Tohoku Daigaku Senko Seiren Kenkyushu Iho,* Vol 38, 1982, p 107-118 (in Japanese)
58. M.R. Baren and N.A. Gokcen, Thermodynamic Properties of S in Fe, Co, Ni and Their Binary Alloys, *Symp. Ext. Process Metall. Meet., Metall. Soc. AIME,* Warrendale, PA, 1983, p 41-56
59. O.A. Kapustin and V.A. Bryukvin, Determination of Sulfur Vapor Pressure Over Sulfide Melts, *Russ. Metall.,* 1988, p 37-41
60. R.Y. Lin, H. Ipser, and Y.A. Chang, Activity of Sulfur in Pyrrhotite at 1073 K, *Metall. Trans. B,* Vol 8, 1977, p 345-346
61. K.-C. Hsieh, "The Thermodynamics and Phase Equilibria of the Fe-Ni-S-O System," Ph.D. dissertation, University of Wisconsin-Madison, 1983
62. T. Rosenqvist, A Thermodynamic Study of the Iron, Cobalt and Nickel Sulphides, *J. Iron Steel Inst.,* Vol 176, 1954, p 37-57
63. E.T. Turkdogan, Fe-S System: Part I. Growth Rate of FeS on Fe and Diffusivities of Fe in FeS, *Trans. AIME,* Vol 242, 1968, p 1665-1672
64. K. Sudo, Fundamental Researches on Smelting of Sulphide Ores, Part II: On the Equilibrium in the Reduction of Solid FeS by Hydrogen Gas, *Sci. Rep. Res. Inst. Tohoku Univ., Ser. A,* Vol 2, Tohoku University, Japan, 1950, p 312-317
65. D. Ferro, V. Piacente, and P. Scardala, Decomposition Enthalpies of Iron Sulfides, *J. Chem. Thermodyn.,* Vol 21, 1989, p 483-494
66. A.D. Pelton, S.A. Degterov, G. Eriksson, C. Robelin, and Y. Dessureault, The Modified Quasichemical Model I—Binary Solutions, *Metall. Trans. B,* Vol 31, 2000, p 651-659
67. A.D. Pelton and M. Blander, Thermodynamic Analysis of Ordered Liquid Solutions by a Modified Quasichemical Approach—Application to Silicate Slags, *Metall. Trans. B,* Vol 17, 1986, p 805-815
68. A.D. Pelton and P. Chartrand, The Modified Quasichemical Model, Part II: Multicomponent Solutions, *Metall. Trans. A,* Vol 32, 2001, p 1355-1360
69. P. Villars, A. Prince, and H. Okamoto, *Handbook of Ternary Alloy Phase Diagrams,* ASM International, 1995, p 887-891
70. P. Waldner and H. Ipser, The Nonstoichiometric ξ-Ni_2In Phase with $B8_2$-Structure: Thermodynamic Modeling, *Intermetallics,* Vol 10, 2002, p 485-491
71. M. Hillert and L.I. Staffanson, Regular Solution Model for Stoichiometric Phases and Ionic Melts, *Acta Chem. Scand.,* Vol 24, 1970, p 3618-3626
72. B. Sundman and J. Ågren, A Regular Solution Model for Phases with Several Components and Sublattices, Suitable for Computer Applications, *J. Phys. Chem. Solids,* Vol 42, 1981, p 297-301
73. C.W. Bale, P. Chartrand, S.A. Degterov, G. Eriksson, K. Hack, R.B. Mahfoud, J. Melançon, A.D. Pelton, and S. Petersen, FactSage Thermochemical Software and Databases, *Calphad,* Vol 26, 2002, p 189-228
74. G. Eriksson and K. Hack, ChemSage—A Computer Program for the Calculation of Complex Chemical Equilibria, *Metall. Trans. B,* Vol 21, 1990, p 1013-1023
75. E. Königsberger and G. Eriksson, A New Optimization Routine for ChemSage, *Calphad,* Vol 19, 1995, p 207-214
76. A.T. Dinsdale, SGTE Data for Pure Elements, *Calphad,* Vol 15, 1991, p 317-425
77. K.C. Mills, *Thermodynamic Data for Sulphides, Selenides and Tellurides,* Butterworths, London, 1974, p 292-301
78. L. Cemič and O. J. Kleppa, High Temperature Calorimetry of Sulfide Systems, III: Standard Enthalpies of Formation of Phases in the Systems Fe-Cu-S and Co-S, *Phys. Chem. Miner.,* Vol 16, 1988, p 172-179
79. F. Grønvold, S. Stølen, A.K. Labban, and E.F. Westrum, Thermodynamics of Iron Sulfides. I. Heat Capacity and Thermodynamic Properties of Fe_9S_{10} at Temperatures from 5 K to 740 K, *J. Chem. Thermodyn.,* Vol 23, 1991, p 261-272
80. P. Waldner and A.D. Pelton, Thermodynamic Modeling of the Ni-S System, *Z. Metallkde.,* Vol 95, 2004, p 672-681
81. P. Waldner and A.D. Pelton, Thermodynamic Assessment of the Fe-Ni-S System, *Metall. Mater. Trans. B,* Vol 35, 2004, p 897-907